PCCP

Structure-property relationship of donor-acceptor acridones – An optical, electrochemical and computational study

Journal:	*Physical Chemistry Chemical Physics*
Manuscript ID:	CP-ART-06-2015-003222.R1
Article Type:	Paper
Date Submitted by the Author:	07-Jul-2015

Complete List of Authors:	Theriault, Kim; University of Calgary, Chemistry Radford, Chase; University of Calgary, Chemistry Parvez, Masood; University of Calgary, Chemistry Heyne, Belinda; University of Calgary, Chemistry Sutherland, Todd; University of Calgary, Chemistry

Journal Name

ARTICLE

Structure-property relationship of donor-acceptor acridones – An optical, electrochemical and computational study

Received 00th January 20xx,
Accepted 00th January 20xx

DOI: 10.1039/x0xx00000x

www.rsc.org/

K. D. Thériault, C. Radford, M. Parvez, B. Heyne, and T. C. Sutherland*

The synthesis of two neutral acridone derivatives were carried out to design media sensitive chromophores by taking advantage of intramolecular charge transfer (ICT) features. The molecules comprised two different donor-acceptor-donor triads, with absorption maxima at 425 nm and 520 nm, for the ketone and dicyanomethylene derivatives, respectively. The ketone variant exhibited fluorescence at room temperature, whereas the dicyanomethylene derivative was only emissive in frozen hexane. The ketone emission was highly solvatochromic, with Stokes shifts that ranged from 5000 cm^{-1} to 10000 cm^{-1}. Electrochemically, both compounds displayed similar oxidation potentials at approximately 0.35 V versus ferrocene/ferrocenium, which was anticipated since both systems employ the same ethynylaniline donor portion of the molecule, whereas only the 9-dicyanomethylene derivative showed a reduction peak at -1.5 V vs Fc/Fc+. Additional spectroelectro-chemical experiments supported a delocalized cationic charge on the ethynylaniline fragments during oxidation and that during electrochemical reduction the dicyanomethylene moieties show localized anionic charge. All of the experimental observations are finally compared to DFT, TDDFT and NICS(0) computations to gain insight into the transitions involved and deduce the role of the acridone core in stabilizing its oxidized and reduced forms.

Introduction

Acridone **1**, shown in Figure 1, is a well-known structural core in the natural products community and its derivatives have found uses as anti-cancer drugs,[1] inhibitors of multi-drug resistance,[2] fluorescent markers[3] and colorimetric sensors.[4] Despite the wealth of synthetic methodology aimed at targets for medical applications, there are few syntheses of pi-conjugated acridones for organic materials applications. The acridone core is highly fluorescent with quantum yields of 0.55[5] and an emission color that is sensitive to its environment, which are both desirable attributes relevant to designing media-sensitive chromophores for biolabeling purposes. From an organic materials perspective, acridone is considered an electron-deficient aryl system, which after installation of π-conjugated electron donors could lead to candidate donor-acceptor (D-A) chromophores. Covalently linked π-conjugated D-A chromophores often participate in intramolecular charge transfer (ICT) excitations, which leads to media sensitive absorption and/or emission properties. The research field of D-A chromophores has been extensively reviewed for fundamental understanding of intramolecular charge transfer[6-9] and applications in optoelectronics,[10] sensors,[11] and photosensitizers.[12]

Acridone is a commercially available and modifiable building block but few reports have expanded this system to exploit its optical and electronic properties toward organic materials applications.[13-16] This literature gap is surprising because its π-extended congener, quinacridone, has been studied extensively and has proven to be a robust pigment molecule with low HOMO-LUMO energy gaps.[17, 18] Previously, we reported an electron donating organic system using a phenothiazine core[19] however, their optical HOMO-LUMO energy gap was quite large (3.2 eV), limiting their use as visible-light chromophores. Here, we conceptually replace the electron-rich thiazine ring with an electron-deficient pyridinone ring with the goal of achieving a lower energy LUMO. Installation of an electron deficient ring should lead to stronger acceptor character on the core acridone while appended ethynylanilines should destabilize the HOMO energy and open the potential for ICT bands between donor (D) and acceptor (A) groups for organic materials applications.

Acridone is most commonly functionalized at the 2,7-position, as well as the 9- and N- positions, as indicated in

Department of Chemistry
University of Calgary
2500 University Drive NW
Calgary, Alberta T2N 1N4 (Canada)
E-mail: todd.sutherland@ucalgary.ca

Electronic Supplementary Information (ESI) available: FTIR spectra, cyclic voltammetry, electrochemistry, spectroelectrochemistry, solvatochromism, crystal structures (CCDC 1056378-1056379), NMR spectra and DFT results. . See DOI: 10.1039/x0xx00000x

Figure 1. There are only three reports of bis-2,7-ethynyl-functionalized acridone structures[13, 20, 21] and of these only one report of a 9-dicyanomethylene functionalized derivative.[13] Wong and co-workers employed the bis-2,7-ethynyl-acridone core for use in metallo-polymers and report optical gaps as low as 2.1 eV (590 nm onset). These promising optical properties for polymers encouraged us to design an analogous small molecule, metal free, acridone scaffold that would have favorable optical gaps.

Structurally, the acridone core tends to be planar,[22] whereas the 9-dicyanomethylene derivative adopts a bent-butterfly shape[23] and the effect of structure on optical properties is explored. In addition, we investigate the installation of strong electron donating groups to the 2,7-positions of acridone to affect the HOMO energy and quantify the LUMO energy level tuning by comparing ketone and dicyanomethylene derivatives. The resulting electronic and optical properties of two D-A-D triads are presented. An extensive computational study of these D-A-D triads support the experimental data and help to elucidate the charge delocalization and the inherent stability of their charged species. This can lead to a better understanding of the acridone D-A-D systems once they are oxidized or reduced and provide a road to the rational design of materials for organic electronics.[24, 25]

Results and Discussion

Synthesis and structure

The syntheses of the two D-A-D chromophores are shown in Figure 1. Acridone, **1**, was *N*-alkylated with 1-bromodecane provided 10-decyl-9-acridone, **2a** in 75% yield. Bromination of **2a** with NBS following literature methods[26] gave 2,7-dibromoacridone **3a** in 89% yield. Knoevenagel condensations of **2a** and **3a** with malononitrile[13] resulted in the analogous dicyanomethylene precursors **2b** and **3b**, respectively, in approximately 70% yield. Both dibromo-precursors, **3a** and **3b**, were subjected to Sonogashira cross coupling conditions with *N*-dialkylated-ethynylaniline[19, 27] to produce the two D-A-D chromophores **4a** and **4b**, in 58% and 73% yield, respectively. Single crystals of the final compounds were elusive. Due to the length and number of alkyl chains, which resulted in viscous oils, neither **4a** nor **4b** exhibited phase transitions in differential scanning calorimetry and only showed decomposition at temperatures of roughly 350 °C as assessed by thermal gravimetric analysis. Precursors **2a** and **2b,** however, did yield single crystals suitable for x-ray analysis, which were then used as comparator core structures with computational methods to support the selection of functional and basis set.

Ortep representations of the crystal structures of **2a** and **2b** are shown in Figure 2 with ellipsoids drawn at the 50% probability level. The most notable difference between structures **2a** and **2b** arises from the deviation from planarity about the central heterocyclic ring. Ketone **2a** is nearly planar about the dibenzannulated pyridone ring, as opposed to the butterfly-shaped dicyanomethylene variant, **2b**, which shows an angle of 153° between intersecting planes of the benzo fused rings. Of particular interest is the packing arrangement of **2a** and **2b** shown in the SI. Molecules of **2a** form heat-to-tail dimers through aryl-aryl interactions that are arranged in a herringbone pattern. Conversely, molecules of **2b** form sheets of parallel-staggered stacks segregated by alkyl domains. These non-polar alkyl domains electronically isolate each sheet and could lead to insight on charge pathways through the bulk material. The optimized ground-state structures, using DFT methods [B3LYP 6-31G+(d)], accurately modeled both crystal structures **2a** and **2b**, lending support to the computational method chosen.

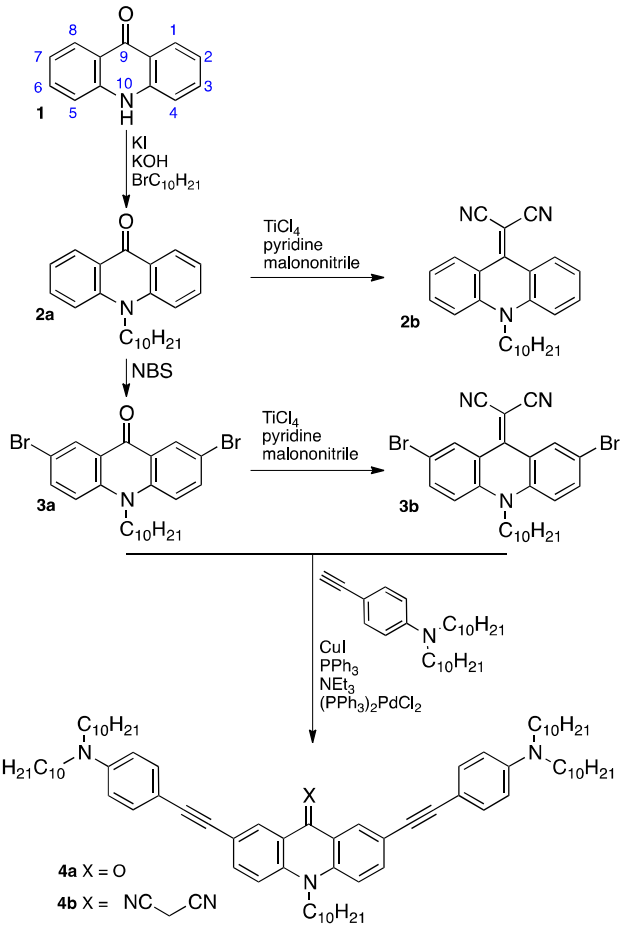

Figure 1. Synthesis of 4a, 4b.

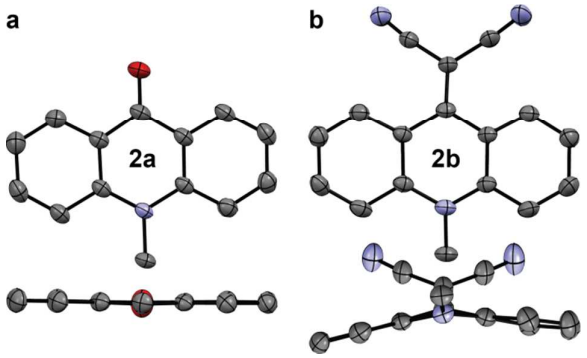

Figure 2. ORTEP representations at 50% probability of a) **2a** b) **2b** with the *n*-decyl chains truncated to methylene and hydrogens atoms omitted. Blue represents nitrogen, red represents oxygen.

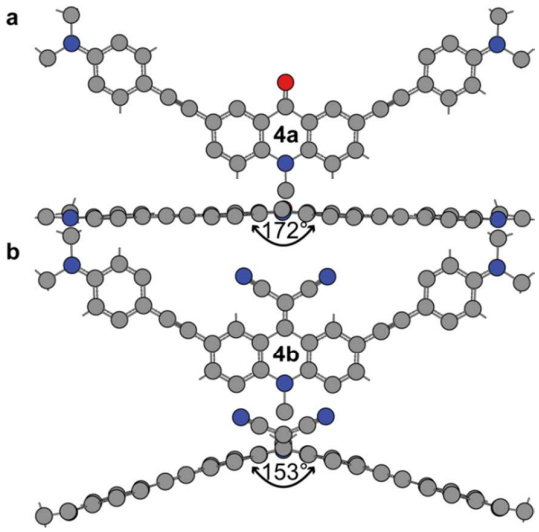

Figure 3. Calculated ground state structures of a) **4a** and b) **4b** showing the angle of the annulated benzo rings (DFT B3LYP 6-31G+(d)).

For comparison, optimized structures of **4a** and **4b** are shown in Figure 3 using the same computational method. It was found computationally that analogous to **2a**, the core of π-extended compound **4a** maintains its planarity, while the core of **4b** is bent in a similar fashion to parent compound **2b**. In a previous report[19] of a related compound whereby the carbonyl of **4a** was replaced with a sulfoxide, the ground state and excited state structures showed large changes. The same computational study of ground state and excited state optimized geometries were carried out here with **4a** and **4b** and showed minimal structural change in the ground versus excited states. The TD-DFT results of the absorption and emission energies, in nanometers, are shown in the ESI and will be discussed below.

Optical and electrochemical properties

The absorption and emission spectra of **4a** and **4b** in hexane are shown in Figure 4a and all optical transitions were compared to TD-DFT computations. A strong absorption at λ_{max} = 368 nm in hexane with a molar absorptivity above 10^5 $M^{-1}cm^{-1}$ is observed for **4a**, consistent with a π-π* transition.[28] This π-π* absorption correlates with the calculated dominant π-π* transition at 412 nm from the HOMO to LUMO+1, as shown in Figure 4b, with an oscillator strength of 2.1. In addition, **4a** also presents smaller absorption features at approximately 450 nm (λ_{onset} = 460 nm, 2.7eV), which is ascribed to an ICT transition that was calculated as the HOMO-1 to LUMO transition with an oscillator strength of 0.15. As seen in Figure 4b, the HOMO-1 orbital coefficients are localized to the aniline fragments, whereas the LUMO coefficients are localized on the acridone core, consistent with the ICT assignment. In hexane, acridone **4a** shows a fluorescence peak at 454 nm and a vibronic shoulder at 478 nm. Comparatively, *N*-methylated acridone exhibits an absorption peak at 393 nm and is fluorescent at 410 nm,[29] which illustrates that the appended ethynyl-anilines lower the optical band gap. A related π-conjugated 2,7-bisthienyl-acridone[30] shows an absorption band at 425 nm, suggesting the ethynylanilines are stronger donors than thiophene and further destabilized the HOMO energy level. The emission spectra in hexane of both **4a** and **4b** are shown in Figure 4a. Acridone **4a** is fluorescent at room temperature in a variety of solvents. In room temperature hexane, **4a** has a Stokes shift of 5000 cm^{-1} with a vibronic shoulder, suggesting a somewhat rigid ground-state structure.[31] To probe the nature of the ICT band in **4a**, a variety of solvents were screened and their effects on both absorption and emission spectra are described below.

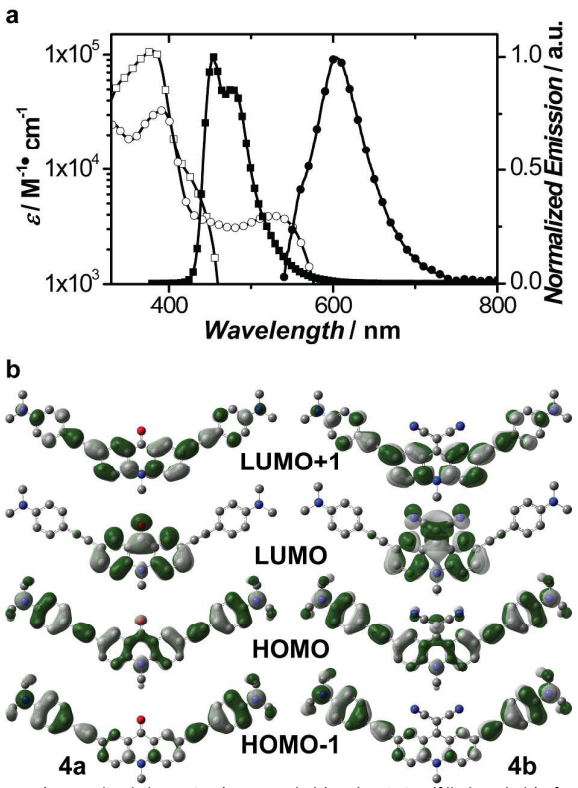

Figure 4. a) Normalized absorption (open symbols) and emission (filled symbols) of **4a** (squares) and **4b** (circles) in hexane. Note, emission spectrum of **4b** was only obtainable in frozen hexane matrix. b) DFT calculated frontier MOs of **4a** and **4b** (B3LYP 6-31G+(d)).

Dicyanomethylene **4b** has a 14 nm red-shift in the π-π* absorption (λ_{max} = 382 nm) relative to the keto analogue **4a**. Similar to **4a**, this optical transition calculated at 419 nm corresponds to the HOMO to LUMO+1 transition with a slightly weaker oscillator strength of 1.8. The stronger electron withdrawing dicyanomethylene moiety elicited a lower energy, broad ICT band centered at λ_{max} = 518 nm, with an onset of 556 nm (2.1 eV), which was determined computationally at 590 nm as a HOMO-1 to LUMO transition with an oscillator strength of 0.15. Clearly, the stronger acceptor character coupled with the aniline donors result in a dramatic bathochromic absorption shift. the emission from **4b** was only obtained in a frozen hexane matrix as fluorescence was absent at room temperature regardless of solvent, common with low energy ICT absorptions. This lack of room temperature fluorescence suggests facile thermal relaxation is occurring in **4b**,[32-34] including but not limited to torsional induced non-radiative decay due to the non-coplanar excited state structure,[35-37] and rotation induced non-radiative decay via the aniline C-N bond and/or the dicyanomethylene C=C bond.[38, 39] In a frozen hexane matrix, dicyanomethylene **4b** shows a Stokes shift of 2700 cm^{-1}.

The modest Stokes shift of ketone **4a** in hexane was much larger in dichloromethane at 8300 cm^{-1} and is further evidence of an ICT transition assignment. Clearly, the fluorescence properties of **4a** are strongly solvatochromic, which is highlighted in Figure 5a. Of the solvents screened, the Stokes shift varied between 5000 cm^{-1} to 10000 cm^{-1}, which is consistent with an ICT mechanism, as determined from the difference in energy from the strong π-π* absorption peak to the highest energy emission peak. The emission and Stokes shift data were fit to several solvent models, including the Lippert-Mataga,[40, 41] $E_T(30)$[42] and multi-parameter solvent model by Catalan,[43] all of which resulted in similar linear correlation values. The solvatochromic behavior clearly suggests the excited state is more polar than the ground state. The Lippert-Mataga plot, shown in Figure 5b, enables the determination of the excited state dipole change ($\Delta\mu$). The Onsager cavity radius of **4a** was determined by calculating the volume of the π-conjugated portion of **4a** and assuming a spherical shape. The volumetric approach results in an estimated Onsager cavity radius of 5 Å, which gives rise to a $\Delta\mu$ value of 13.8 D for **4a**. Computationally, the change in dipole from the ground (3.51 D) to excited (2.79 D) state was 0.72 D, which highlights the limitation of DFT methods to accurately model ICT transitions.[44-46] The absorption peaks of **4a** did not show a linear relation to any of the above three solvent models, suggesting specific solvent interactions in the ground state. Interestingly, in the Catalan multi-parameter fit, only a single term, solvent dipolarity, had influence on linearizing the emission data of **4a** and literature has shown that solvent dipolarity is correlated to the $E_T(30)$ scale, which models empirically ICT transitions.[43]

Electrochemically, acridone derivatives **4a** and **4b** exhibit low irreversible oxidation potentials at 0.34 V and 0.37 V (vs. Fc/Fc^+), respectively, as expected for π-extended anilines, and result in approximate HOMO energy values of -5.1 eV and -5.2 eV for **4a** and **4b**, respectively. Furthermore, both **4a** and **4b** show a second irreversible oxidation peak at 0.70 V and 0.72 V, respectively. To compare, an *N*-phenyl acridone derivative has an oxidation potential of approximately 1.3 V vs Fc/Fc^+.[16] Clearly, the appended bis-2,7-ethynylanilines have increased the HOMO energy levels drastically over acridone. Under reductive potentials, ketone **4a** did not show a reducing peak within the solvent / electrolyte stability window, whereas dinitrile derivative **4b** displayed a quasi-reversible reduction peak at -1.47 V vs Fc/Fc^+. For comparison, an *N*-phenyl acridone derivative[16] shows a reduction potential of approximately -2.0 V (vs Fc/Fc^+), again highlighting the impact of installing the dicyanomethylene to lower the LUMO energy by approximately 0.5 eV. The reduction peak in **4b** provides an estimated LUMO energy value of -3.3 eV, compared to an estimated LUMO energy value of -3.0 eV for **4a**, based on oxidation potential and absorption onset values. The electrochemically approximated HOMO-LUMO energy gap of 1.9 eV for **4b** compares favorably with the optically determined energy gap of 2.1 eV and highlights the effect of electron-withdrawing properties on acridone.

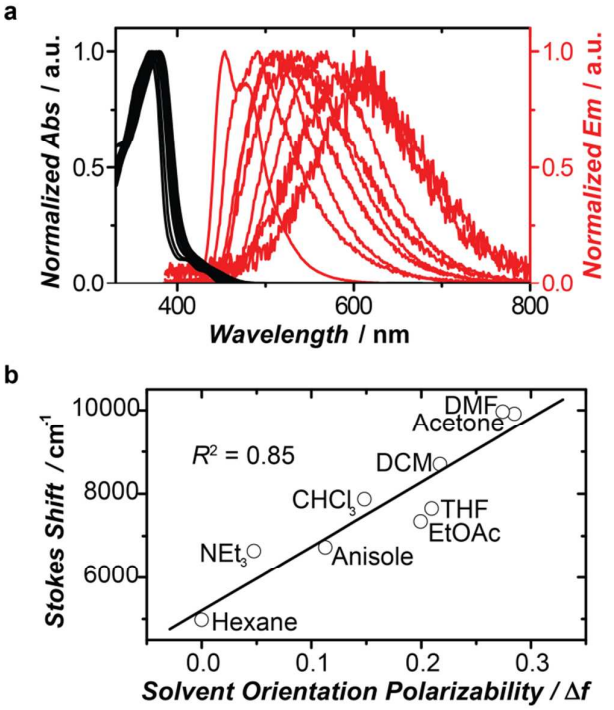

Figure 5. a) Absorption (black) and emission (red) spectra of **4a** in hexanes, triethylamine, anisole, ethyl acetate, tetrahydrofuran, chloroform, dichloromethane, acetone, and dimethylformamide. b) Lippert-Mataga plot of the Stokes shift in the various solvents.

Spectroelectrochemistry

While applying an oxidizing potential at the first oxidation peak potential to a solution containing electrolyte and acridone **4a,** a new low energy absorption peak at 650 nm grew in with a concomitant decrease in the intense π-π* transition at 391 nm, as shown in the top panel of Figure 6. The broad low energy absorption is characteristic of a π-

delocalized cation. The clear isosbestic points indicate the cation is somewhat stable and does not degrade into optically active species. This was reflected in the change in IR frequencies of **4a** when the species was oxidized, as the alkyne and aromatic carbon stretching frequencies indicated a more delocalized quinoidal form to stabilize the positive charge. The spectro-electrochemical IR spectra of the charged species and further discussion can be found in the ESI.

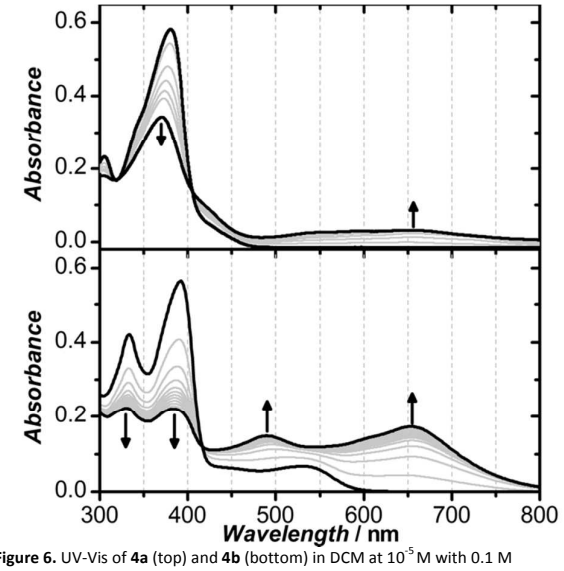

Figure 6. UV-Vis of **4a** (top) and **4b** (bottom) in DCM at 10^{-5} M with 0.1 M tetrabutylammonium tetrafluoroborate and an applied oxidative potential recorded once per minute.

Dicyanomethylene **4b** was subjected to the same spectro-electrochemical assessment, resulting in similar optical features appearing during the oxidation, although at longer wavelengths (Figure 6, bottom). The characteristic π-delocalized cation has an absorption onset beyond 800 nm and a marked decrease in the strong π-π* transition. Upon reduction of **4b**, the first few scans taken at one-minute intervals show a decrease in the ICT band, which is expected since the molecule transformed from a D-A-D triad to a D-D-D triad, essentially shutting down the ICT transition. However, no isosbestic points were observed in the electrochemically reduced spectra of **4b**, suggesting either anion decomposition occurred to optically active compounds or multiple anionic species were forming concurrently. The IR frequencies of the reduced **4b** species shows a significant increase in the CN bond stretching frequency while the alkyne stretching frequencies are less affected, indicating that the anionic charge is localized about the malononitrile moiety, further complementing the decrease in the optically observed ICT transition.

Additional insight into the spectroelectrochemical experimental results can be gained from computations. Optimized structures of **4a** and **4b** and their associated oxidized and reduced versions were determined using the same DFT methods previously described in addition to an aromaticity index, NICS(0) for all rings. For this assessment, only singlet states were considered. Electron density maps of **4a** and **4b** in their 2+, 1+, 0, 1- and 2- charge states are found in the ESI. For ketone **4a**, regardless of the charge, the structures remain essentially planar. Upon one- or two-electron oxidation, the cationic charge is delocalized throughout the aniline backbone leading to well-distributed charge density and is indicative of a stable cation and a candidate electron donor material. The experimentally observed long wavelength absorption band that grows in during oxidation supports the highly delocalized cationic charge. Conversely, the one- and two-electron reduced structures show anionic charge localized to the keto functional group. Dicyanomethylene **4b** exhibits the same delocalized cation structures as **4a** whilst maintaining the bent, butterfly-shape. However, upon reduction the calculated structures of **4b** become planar, as illustrated in Figure 7. Upon the first reduction, the core flattens and the appended dicyanomethylene twists out of plane, presumably due to the build-up of anionic charge on the C=C bond of the dicyanomethylene, reducing its bond order. This reduced bond-order is more pronounced in the dianion structure, as the dicyanomethylene moiety is nearly perpendicular to the aromatic system. These structural changes upon reduction have been reported with anthraquinone derivatives.[47]

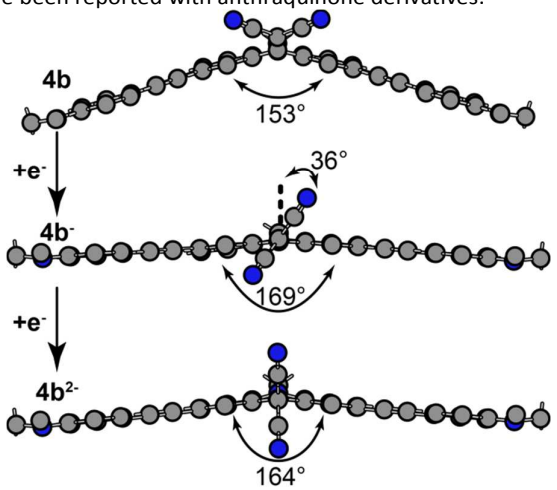

Figure 7. Calculated structures of neutral, anionic and dianionic forms of **4b** (DFT B3LYP 6-31G+(d)).

Of particular interest for stability purposes, is the computationally derived index of aromaticity. Aromaticity was assessed for all rings present in **4a** and **4b** using the NICS(0) method.[48, 49] This assessment of the acridone core gives insight into how the core could either stabilize or destabilize the cationic or anionic species in organic semiconducting applications. A change in the level of aromaticity can give insight into possible ease of reduction or oxidation and indicate stabilities of oxidized or reduced compounds. To establish a basis of comparison, **4a** and **4b** were subjected to NICS(0) calculations in their neutral states, as shown in Figure 8. For discussion purposes, the following ranges of NICS(0) values are arbitrarily used as indices to assess aromatic character: anti-aromatic > 5; non-aromatic 5 to 0; somewhat aromatic 0 to -5; aromatic < -5 and are color coded into Figure 8. In neutral forms, both **4a** and **4b** share similar aromatic

indices such that the central pyridone ring is somewhat aromatic while both the aniline and benzo-fused rings are aromatic. Upon oxidation to the monocation, the pyridone ring of acridone **4a** becomes non-aromatic, the anilines become somewhat aromatic and the benzo-fused rings maintain their aromaticity. These aromaticity results of the cation compound are consistent with a more quinoidal form of the terminal ethynyl anilines. This quinoidal form can be observed from the optimized structures (ESI) of the cations, as there is a greater disparity between alternating bond lengths in the aniline rings of the oxidized structures. Dicyanomethylene derivative **4b** is similar to **4a** with respect to aromatic character, except the central pyridine ring maintains its somewhat aromatic character as the monocation. Upon reduction of acridone **4a** to the monoanion, the central pyridone ring adopts antiaromatic character, which could explain the large negative potential (beyond the electrochemical solvent window) required to observe this species. In concert, the benzo-fused rings become non-aromatic while the terminal ethynyl anilines maintain their aromaticity. The heterocyclic ring of dicyano **4b** becomes anti-aromatic upon reduction but the benzo-fused rings are still somewhat aromatic, suggesting a more stabilized anion compared to structure **4a**. Comparing the electrochemical oxidation and reduction potentials of both **4a** and **4b** to their respective aromaticity index, it is clear that the oxidized species is sufficiently delocalized and has minimal effect on the molecular aromaticity. Conversely, upon reduction, there is a loss of aromatic character to the acridone core, which supports both the large potential required to reduce **4b** and its observed electrochemical quasireversibilty.

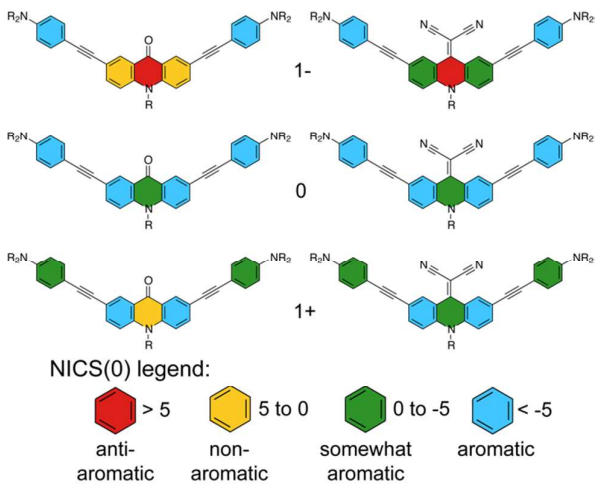

Figure 8. NICS(0) calculation of **4a** and **4b** in various degrees of oxidation/reduction (DFT B3LYP 6-31G+(d)).

Conclusions

We report a pair of donor-acceptor-donor triads based on a readily available acridone core as potential building blocks for organic semi-conductors. The D-A-D compounds exhibited intra-molecular charge transfer (ICT) absorptions and were emissive. The fluorescence spectrum of the acridone derivative was strongly solvatochromic, consistent with an ICT transition and permitted a Lippert-Mataga analysis resulting in a transition dipole moment of 13.8 D. The stronger electron-accepting dicyanomethylene derivative did show an electrochemical reduction, whereas the parent acridone compound did not reduce electrochemically within the solvent stability window. Both compounds oxidize irreversibly at low potentials. The two triads were subjected to spectroelectrochemical experiments, which confirmed a delocalized cation upon oxidation. Finally, the compounds and their respective anions and cations were compared to computational assessments to provide insights into aromaticity changes during redox reactions.

Acknowledgements

The authors thank NSERC of Canada (RGPIN/04444-2014) for funding and KDT acknowledges NSERC and AITF for scholarship support.

Experimental Section

Materials

All solvents used were purchased from either Aldrich or Fischer and used as received except for the following: triethylamine and pyridine were distilled from CaH_2 and stored over sieves; THF and DMF were stored over sieves. All reagents were purchased from Aldrich and used as received except: K_2CO_3, H_2SO_4 and KOH purchased from EMD; KI and aniline purchased from BDH; and TMS acetylene purchased from Oakwood. Acridone was prepared in our lab following literature procedure. [50] Column chromatography was performed on SiliCycle Silica-Flash P60 silica gel (230-400 mesh). Thin-layer chromatography was carried out on Merck silica gel F_{254} aluminium-backed TLC plates.

General

NMR spectra were recorded on a Bruker 400MHz spectrometer and referenced to residual $CHCl_3$ in $CDCl_3$ (^{1}H 7.26ppm, ^{13}C 77.00) or residual DMSO-D_5H in DMSO-D_6 (^{1}H 2.50ppm). All mass spectra were recorded with a Bruker Daltonics Autoflex MALDI-TOF spectrometer. FTIR spectra were recorded in diffuse reflectance mode with drop-cast films on ground KBr on a Varian FTS-7000 spectrometer. All UV/Vis spectra were collected on a Cary 5000 UV-Vis-NIR spectrophotometer in dual beam mode, using a Starna Inc. quartz semi-micro spectrophotometer cell. All emission spectra were recorded using a PTI Quanta Master spectrofluorimeter operated in CW mode, using a 1 cm × 1 cm path length quartz cell fabricated in house. All differential pulse voltammetry (DPV) and cyclic voltammetry (CV) experiments were carried out on an Autolab PGSTAT302 potentiostat that was controlled by a PC running Autolabs's GPES v 4.9 software in a temperature-controlled, three-electrode cell (15 mL). The working electrode was a Pt button, the reference electrode was a silver wire, and the counter electrode was a platinum wire. All potentials were referenced

to the ferrocene/ferricenium redox couple. Each DPV experiment consisted of approximately 5 mM redox active product dissolved in 0.1 M tetrabutylammonium tetrafluoroborate in degassed dichloromethane, maintaining an argon blanket during the entire experiment. Spectroelectrochemical spectra were recorded with the Cary 5000 and Varian FTS-7000 spectrometers for the UV-Vis and the IR respectively, linked to a CHI 650 potentiostat using a thin layer cell (OTTLE) with a Pt mesh working electrode in the beam path, a Pt wire counter electrode, and a Ag wire reference electrode; electrolyte and solvent were used as above.

Synthesis

Formation of 10-decylacrid-9-one (**2a**): In a round bottom flask, **1** (0.9974 g, 5.109 mmol), potassium iodide (0.8530 g, 5.133 mmol), and potassium hydroxide (0.5000 g, 8.911 mmol) were suspended in THF (20 mL) and stirred at 40 °C for one hour. 1-bromodecane (2.11 mL, 10.20 mmol) was then added and the reaction was stirred at 40 °C for four days. After completion, the solvent was removed under reduced pressure before reconstituting the mixture in dichloromethane. The organic layer was washed with water then dried with magnesium sulfate. After removal of the solvent in vacuo, the crude product was purified by silica gel chromatography (hexanes : ethyl acetate (4:1)) to afford a mixture of two isomers. The product was then isolated by crystallization from ethanol to afford **2a** as yellow crystals (1.278 g, 3.809 mmol, 75% yield). ^{1}H NMR (400 MHz, Chloroform-*d*) δ 8.58 (d, *J* = 8.0 Hz, 2H), 7.72 (t, *J* = 7.8 Hz, 2H), 7.48 (d, *J* = 8.7 Hz, 2H), 7.29 (t, *J* = 7.4 Hz, 2H), 4.32 (t, *J* = 8.7, 4.1 Hz, 2H), 1.91 (p, 2H), 1.55 (p, *J* = 7.1 Hz, 2H), 1.44 (p, *J* = 6.6 Hz, 2H), 1.39 – 1.24 (m, 10H), 0.89 (t, 3H). ^{13}C NMR (101 MHz, Chloroform-d) δ 178.09, 141.92, 133.96, 128.13, 122.65, 121.28, 114.67, 46.37, 32.00, 29.73, 29.65, 29.50, 29.42, 27.31, 27.07, 22.80, 14.24. MS (MALDI HRMS, HCCA) *m/z* calcd for $C_{23}H_{29}NO$ + H: 336.2322; found 336.2336.

Formation of 2,7-dibromo-10-decylacrid-9-one (**3a**): In a round bottom flask, **2a** (0.2.3879 g, 7.118 mmol) was dissolved in DMF (120 mL), then NBS (3.1671 g, 17.795 mmol) was added to the mixture in one portion. The solution was heated to 80 °C overnight, after which the reaction became red in color. The reaction was quenched with water and the solvents were removed in vacuo. The mixture was reconstituted in DCM, washed with water and the organic layer was dried with magnesium sulfate. The crude product was then purified by silica gel column chromatography (DCM : hexanes (6:1)) to afford **3a** as a bright yellow powder. (3.1380 g, 6.347 mmol, 89% yield). ^{1}H NMR (400 MHz, Chloroform-*d*) δ 8.65 (d, *J* = 2.5 Hz, 2H), 7.79 (dd, *J* = 9.2, 2.5 Hz, 2H), 7.37 (d, *J* = 9.2 Hz, 2H), 4.29 (t, 2H), 1.90 (p, *J* = 7.8 Hz, 2H), 1.59 – 1.49 (m, 2H), 1.44 (p, *J* = 14.7, 7.1 Hz, 2H), 1.37 – 1.23 (m, 10H), 0.90 (t, *J* = 6.8 Hz, 3H). ^{13}C NMR (101 MHz, Chloroform-*d*) δ 175.71, 140.53, 137.08, 130.54, 123.82, 116.88, 115.13, 46.75, 32.01, 29.70, 29.64, 29.48, 29.42, 27.31, 27.01, 22.82, 14.26. MS (MALDI HRMS, HCCA) *m/z* calcd for $C_{23}H_{27}NOBr_2$ + H: 492.0532; found 492.0515.

Formation of 2-(2,7-dibromo-10-decylacridin-9-ylidene)-malononitrile (**3b**): In a Schlenk flask, **3a** (0.3067 g, 0.6218 mmol) was heated under vacuum to remove trace water then purged with nitrogen. Dry pyridine (15mL) was added and the solution was stirred until dissolved then cooled in an ice bath. Titanium (IV) chloride (0.204 mL, 1.86 mmol) was then added over 10 minutes, after which a solution of malononitrile (0.1230 g, 1.865 mmol) dissolved in dry pyridine (10 mL) was added drop wise. The reaction mixture was heated to reflux overnight to afford a deep red colored solution. After removal of pyridine in vacuo, the mixture was reconstituted in DCM, washed with water and dried with magnesium sulfate. The crude product was subjected to silica gel column chromatography (DCM : Hexanes (6:1)), and the collected product was recrystallized in hexanes to afford **3b** as a bright orange powder (0.2332 g, 0.4308 mmol, 70% yield). ^{1}H NMR (300 MHz, Chloroform-*d*) δ 8.60 (d, *J* = 2.2 Hz, 2H), 7.77 (dd, *J* = 9.2, 2.3 Hz, 2H), 7.33 (d, *J* = 9.2 Hz, 2H), 4.23 (t, 2H), 1.90 (p, *J* = 7.6 Hz, 2H), 1.53 – 1.38 (m, 4H), 1.38 – 1.17 (m, 10H), 0.89 (t, *J* = 6.3 Hz, 3H). ^{13}C NMR (101 MHz, $CDCl_3$) δ 153.21, 137.81, 136.58, 129.43, 119.46, 116.46, 116.13, 115.07, 77.37, 48.38, 32.00, 29.66, 29.62, 29.41, 29.35, 27.01, 26.93, 22.82, 14.25. MS (MALDI HRMS, Neat) *m/z* calcd for $C_{26}H_{27}N_3Br_2$ + H: 540.065; found 540.062.

Formation of 2-(10-decylacridin-9-ylidene)malononitrile (**2b**): In a Schlenk flask containing molecular sieves, **2a** (0.4975 g, 1.483 mmol) was added and any trace water was removed in vacuo prior to purging the flask with nitrogen. Dry pyridine (40 mL) was added and the mixture was stirred and cooled in an ice bath. Once cool, titanium (IV) chloride (0.49 mL, 4.449 mmol) was added over 30 minutes then a solution of malononitrile (0.4898 g, 7.415 mmol) in dry pyridine (10 mL) was added drop wise. After refluxing overnight, the reaction mixture was cooled in an ice bath, additional titanium (IV) chloride (0.33 mL, 3.01 mmol) and malononitrile (0.4898 g, 7.415 mmol) solution in dry pyridine (10 mL) was added to the reaction mixture, and was refluxed overnight. The reaction mixture was then cooled and filtered through a silica gel plug using ethyl acetate as eluent to collect the orange colored product. The solvent was removed in vacuo and the crude product was purified by silica gel column chromatography (hexanes : ethyl acetate (4:1)). Recrystallizing the orange product from ethanol yielded **2b** as bright orange crystals (0.3246 g, 0.8470 mmol, 57% yield). ^{1}H NMR (400 MHz, Chloroform-*d*) δ 8.55 (dd, *J* = 8.3, 1.4 Hz, 2H), 7.70 (td, *J* = 8.6, 7.1, 1.5 Hz, 2H), 7.47 (d, *J* = 8.4 Hz, 2H), 7.33 (td, *J* = 8.2, 7.1, 1.0 Hz, 2H), 4.30 (t, 2H), 1.96 (p, *J* = 16.0, 8.0 Hz, 2H), 1.54 – 1.49 (m, 2H), 1.49 – 1.40 (m, 2H), 1.39 – 1.22 (m, 10H), 0.89 (t, 3H). ^{13}C NMR (101 MHz, $CDCl_3$) δ 156.41, 138.92, 133.63, 127.25, 121.97, 118.21, 117.70, 114.31, 68.24, 48.21, 32.01, 29.71, 29.64, 29.42, 29.39, 27.09, 26.97, 22.81, 14.25. MS (MALDI HRMS, Neat) *m/z* calcd for $C_{26}H_{27}N_3^+$: 383.2356; found 383.2353.

Formation of 10-decyl-2,7-bis(4-(N,N-didecylaniline)ethynyl)-acrid-9-one (**4a**): In a Schlenk flask, copper (I) iodide (0.0432 g, 0.227 mmol) and **3a** (0.4313 g, 0.8744 mmol) were heated under vacuum. The flask was purged with nitrogen while

adding triphenylphosphine (0.0504 g, 0.192 mmol) and bistriphenylphosphine palladium (II) chloride (0.0629 g, 0.0896 mmol). Distilled triethylamine (30 mL) was added and the reaction mixture was stirred. A solution of *N*,*N*-didecyl-4-ethynylaniline (0.8266 g, 2.079 mmol) in distilled triethylamine (10 mL) was added over 10 minutes under nitrogen, heating the mixture to 80 °C. After stirring for an hour, the solution was refluxed overnight under nitrogen. The solvent was then removed in vacuo and the mixture was triturated with cold hexanes. The filtrate was reconstituted with DCM, washed with water, dried with magnesium sulfate, and the solvent was removed in vacuo. The crude product was then purified by silica gel column chromatography (hexanes : DCM (1:1)) and triturated with cold pentane to afford **4a** as a viscous bright yellow oil (0.0582 g, 0.0516 mmol, 58% yield). ^{1}H NMR (400 MHz, Chloroform-*d*) δ 8.69 (d, *J* = 2.1 Hz, 2H), 7.78 (dd, 2H), 7.43 (d, *J* = 8.9 Hz, 2H), 7.39 (d, *J* = 8.9 Hz, 4H), 6.58 (d, *J* = 8.9 Hz, 4H), 4.33 (t, 2H), 3.28 (t, 8H), 1.92 (p, 2H), 1.59 (t, 8H), 1.45 (p, 2H), 1.35 – 1.22 (m, 68H), 0.89 (t, *J* = 6.8 Hz, 15H). ^{13}C NMR (101 MHz, Chloroform-*d*) δ 176.79, 148.07, 140.48, 136.35, 133.02, 130.77, 122.45, 117.75, 114.95, 111.35, 108.81, 91.41, 86.49, 51.13, 46.48, 32.05, 32.02, 29.82, 29.73, 29.68, 29.48, 29.45, 27.39, 27.30, 27.05, 22.83, 14.27. MS (MALDI HRMS, HCCA) *m/z* calcd for $C_{79}H_{119}N_3O$ + H: 1126.9426; found 1126.9477.

Formation of 2-(10-decyl-2,7-bis((4-(didecylamino)phenyl)-ethynyl)acridin-9-ylidene)malononitrile (**4b**): In a Schlenk flask, copper (I) iodide (0.011 g, 0.059 mmol) and **3b** (0.1332 g, 0.2951 mmol) were heated under vacuum. The flask was purged with nitrogen while adding triphenylphosphine (0.015 g, 0.059 mmol) and bistriphenylphosphine palladium (II) chloride (0.020 g, 0.030 mmol). Distilled triethylamine (13.5 mL) was added and the reaction mixture was stirred while heating to 80 °C. A solution of *N*,*N*-didecyl-4-ethynylaniline (0.2582 g, 0.649 mmol) in distilled triethylamine (4 mL) was added. The reaction mixture was further heated to 90 °C overnight under nitrogen. The crude product was purified by silica gel chromatography (hexanes:DCM (1:1)) followed by a second silica gel column (hexanes:ethyl acetate (6:1)). The collected product was then triturated with cold pentane to afford **4b** as a viscous dark red oil (0.2545 g, 0.2166 mmol, 73% yield). ^{1}H NMR (400 MHz, Chloroform-*d*) δ 8.58 (d, *J* = 1.8 Hz, 2H), 7.68 (d, *J* = 9.0 Hz, 2H), 7.40 – 7.31 (m, 6H), 6.56 (d, *J* = 9.0 Hz, 4H), 4.39 – 4.13 (m, 2H), 3.39 – 3.20 (m, 8H), 1.90 (p, *J* = 7.7 Hz, 2H), 1.68 – 1.53 (m, 8H), 1.49 (d, *J* = 7.7 Hz, 2H), 1.46 – 1.38 (m, 2H), 1.39 – 1.22 (m, 66H), 1.00 – 0.81 (m, 15H). ^{13}C NMR (101 MHz, $CDCl_3$) δ 154.46, 148.27, 137.46, 136.13, 133.16, 129.08, 118.69, 118.19, 117.34, 114.57, 111.34, 108.39, 92.79, 85.90, 77.36, 68.81, 51.11, 48.16, 32.04, 32.01, 29.81, 29.72, 29.69, 29.67, 29.65, 29.46, 29.43, 29.37, 27.40, 27.30, 26.99, 22.82, 14.24. MS (MALDI HRMS, DCTB) *m/z* calcd for $C_{82}H_{119}N_5^+$: 1173.946; found 1173.949.

Notes and references

1 H. T. Nguyen, M.-C. Lallemand, S. Boutefnouchet, S. Michel and F. o. Tillequin, *Journal of Natural Products*, 2009, **72**, 527-539.
2 P. Singh, J. Kaur, P. Kaur and S. Kaur, *Bioorganic & Medicinal Chemistry*, 2009, **17**, 2423-2427.
3 J. A. Smith, R. West and M. Allen, *Journal of Fluorescence*, 2004, **14**, 151-171.
4 H. Miyaji and J. L. Sessler, *Angewandte Chemie International Edition*, 2001, **40**, 154-157.
5 P. Nikolov, I. Petkova, G. Köhler and S. Stojanov, *Journal of Molecular Structure*, 1998, **448**, 247-254.
6 M. H. V. Huynh, D. M. Dattelbaum and T. J. Meyer, *Coord. Chem. Rev.*, 2005, **249**, 457-483.
7 M. Kivala and F. Diederich, *Acc. Chem. Res.*, 2009, **42**, 235-248.
8 E. Vauthey, *ChemPhysChem*, 2012, **13**, 2001-2011.
9 M. R. Wasielewski, *Acc. Chem. Res.*, 2009, **42**, 1910-1921.
10 T.-D. Kim and K.-S. Lee, *Macromol. Rapid Commun.*, 2015, **36**, 943-958.
11 T. Michinobu, Y. Li and T. Hyakutake, *Phys. Chem. Chem. Phys.*, 2013, **15**, 2623-2631.
12 G. Qian and Z. Y. Wang, *Chem. - Asian J.*, 2010, **5**, 1006-1029.
13 W.-C. Chow, G.-J. Zhou and W.-Y. Wong, *Macromol. Chem. Phys.*, 2007, **208**, 1129–1136.
14 E. M. McGale, R. E. Murray, C. J. McAdam, J. L. Morgan, B. H. Robinson and J. Simpson, *Inorg. Chim. Acta*, 2003, **352**, 129-135.
15 A. A. Vasilev, K. De Mey, I. Asselberghs, K. Clays, B. Champagne, S. E. Angelova, M. I. Spassova, C. Li and K. Müllen, *J. Chem. Phys. C*, 2012, **116**, 22711-22719.
16 D. A. K. Vezzu, J. C. Deaton, M. Shayeghi, Y. Li and S. Huo, *Org. Lett.*, 2009, **11**, 4310-4313.
17 E. D. Głowacki, M. Irimia-Vladu, M. Kaltenbrunner, J. Gąsiorowski, M. S. White, U. Monkowius, G. Romanazzi, G. P. Suranna, P. Mastrorilli, T. Sekitani, S. Bauer, T. Someya, L. Torsi and N. S. Sariciftci, *Adv. Mater. (Weinheim, Ger.)*, 2013, **25**, 1563-1569.
18 M. J. Robb, S.-Y. Ku, F. G. Brunetti and C. J. Hawker, *J. Polym. Sci., Part A: Polym. Chem.*, 2013, **51**, 1263-1271.
19 K. D. Thériault and T. C. Sutherland, *Phys. Chem. Chem. Phys.*, 2014, **16**, 12266-12274.
20 M. Kivala, W. Pisula, S. Wang, A. Mavrinskiy, J.-P. Gisselbrecht, X. Feng and K. Muellen, *Chem. - Eur. J.*, 2013, **19**, 8117-8128.
21 S. Loeffler, J. Luebben, L. Krause, D. Stalke, B. Dittrich and G. H. Clever, *J. Am. Chem. Soc.*, 2015, **137**, 1060-1063.
22 G. D. Potts and W. Jones, *Acta Crystallogr., Sect. C: Cryst. Struct. Commun.*, 1995, **51**, 267-268.
23 T. Takeda, H. Sugihara, Y. Suzuki, J. Kawamata and T. Akutagawa, *J. Org. Chem.*, 2014, **79**, 9669-9677.
24 P. M. Burrezo, X. Zhu, S.-F. Zhu, Q. Yan, J. T. López Navarrete, H. Tsuji, E. Nakamura and J. Casado, *J. Am. Chem. Soc.*, 2015, **137**, 3834-3843.
25 M. Fujitsuka, D. W. Cho, S. Tojo, J. Choi, H.-H. Huang, J.-S. Yang and T. Majima, *The Journal of Physical Chemistry A*, 2014, **118**, 2307-2315.
26 Y. Maegawa, N. Mizoshita, T. Taniab and S. Inagaki, *J. Mater. Chem.*, 2010, **20**, 4399-4403.
27 S. N. Keller, N. L. Veltri and T. C. Sutherland, *Org. Lett.*, 2013, **15**, 4798–4801.
28 S. Nakade, T. Kanzaki, W. Kubo, T. Kitamura, Y. Wada and S. Yanagida, *J. Chem. Phys. B*, 2005, **109**, 3480–3487.
29 A. Boużyk, L. Jóźwiak, A. Y. Kolendo and J. Błażejowski, *Spectrochimica Acta Part A: Molecular and Biomolecular Spectroscopy*, 2003, **59**, 543-558.
30 A. Świst, J. Cabaj, J. Sołoducho, P. Ç. Data and M. Ç. Łapkowski, *Synthetic Metals*, 2013, **180**, 1-8.

31 N. J. Turro, V. Ramamurthy and J. C. Scaiano, *Modern molecular photochemistry of organic molecules*, University Science Books, Sausalito, Calif., 2010.
32 W. A. Donald, R. D. Leib, J. T. O'Brien, M. F. Bush and E. R. Williams, *J. Am. Chem. Soc.*, 2008, **130**, 3371-3381.
33 J. K. R. Thomas, J. T. Lin, M. Velusamy, Y. T. Tao and C. H. Chuen, *Adv. Funct. Mater.*, 2004, **14**, 83-90.
34 M. Zhang, Z. Wu, Q. Wang, Q. Song and Y. Ding, *Mater. Lett.*, 2010, **64**, 2244-2246.
35 M. Belletête, J.-F. Morin, M. Leclerc and G. Durocher, *J. Phys. Chem. A*, 2005, **109**, 6953-6959.
36 D. A. M. Egbe, T. Kietzke, B. Carbonnier, D. Mühlbacher, H.-H. Hörhold, D. Neher and T. Pakula, *Macromolecules (Washington, DC, U. S.)*, 2004, **37**, 8863-8873.
37 D. Oelkrug, A. Tompert, J. Gierschner, H.-J. Egelhaaf, M. Hanack, M. Hohloch and E. Steinhuber, *J. Chem. Phys. B*, 1998, **102**, 1902-1907.
38 L. A. Estrada, X. Cai and D. C. Neckers, *J. Phys. Chem. A*, 2011, **115**, 2184-2195.
39 S. Mqadmi and A. Pollet, *J. Photochem. Photobiol., A*, 1990, **53**, 275-281.
40 E. Lippert, *Z. Elektrochem. Ber. Bunsenges. physik. Chem.*, 1957, **61**, 962-975.
41 N. Mataga, Y. Kaifu and M. Koizumi, *Bull. Chem. Soc. Jpn.*, 1956, **29**, 465-470.
42 C. Reichardt, *Chem. Rev. (Washington, DC, U. S.)*, 1994, **94**, 2319-2358.
43 J. Catalán, *J. Chem. Phys. B*, 2009, **113**, 5951-5960.
44 J. R. Reimers, Z.-L. Cai, A. BiliĆ and N. S. Hush, *Annals of the New York Academy of Sciences*, 2003, **1006**, 235-251.
45 Z.-L. Cai, M. J. Crossley, J. R. Reimers, R. Kobayashi and R. D. Amos, *The Journal of Physical Chemistry B*, 2006, **110**, 15624-15632.
46 P. Dev, S. Agrawal and N. J. English, *The Journal of Chemical Physics*, 2012, **136**, 224301.
47 A. E. Murschell, W. H. Kan, V. Thangadurai and T. C. Sutherland, *Phys. Chem. Chem. Phys.*, 2012, **14**, 4626-4634.
48 M. Bühl and C. van Wüllen, *Chem. Phys. Lett.*, 1995, **247**, 63.
49 P. v. R. Schleyer, C. Maerker, A. Dransfeld, H. Jiao and N. J. R. v. E. Hommes, *J. Am. Chem. Soc.*, 1996, **118**, 6317-6318.
50 Y. Markovich, T. Kudryavtseva, M. Brylev, V. Markovich and K. I., *Russ. J. Gen. Chem.*, 2012, **82**, 149-152.